

CERN-TH/2001-036

IPPP/01/62

DCPT/01/24

December 2001

Revised October 26, 2018

A study of single sneutrino production in association with fermion pairs at polarised photon colliders

Dilip Kumar Ghosh^{a,1} and Stefano Moretti^{b,2}

^a *Department of Physics, National Taiwan University
Taipei, TAIWAN 10617, Republic of China*

^b *CERN Theory Division, CH-1211 Geneva 23, Switzerland*

and

Institute for Particle Physics Phenomenology, University of Durham, Durham DH1 3LE, UK

Abstract

We investigate single sneutrino production in the context of R-parity-violating Supersymmetry at future $\gamma\gamma$ linear colliders. The sneutrino is produced in association with fermion pairs and it is shown that its decays into two further fermions will lead to a clean signal. We also discuss possible Standard Model backgrounds and the effects of beam polarisation.

PACS Nos.: 12.60.Jv, 13.10.+q, 14.80.Ly

¹dghosh@phys.ntu.edu.tw

²Stefano.Moretti@cern.ch

1 Introduction

Supersymmetry (SUSY) is currently the most attractive theoretical framework describing physics beyond the Standard Model (SM). Even the minimal extension of the SM incorporating SUSY (MSSM) predicts a zoo of new particles, which have not yet been observed. One of the major areas of activity in high energy physics today and in the near future is to prove their existence. If SUSY is realised at the electroweak (EW) scale, many of the superparticles should be discovered at next generation hadron colliders, such as Tevatron (Run II, $\sqrt{s_{pp}} = 2$ TeV) at FNAL and the Large Hadron Collider (LHC, $\sqrt{s_{pp}} = 14$ TeV) at CERN. These machines, while having the chance of being the first to access the SUSY domain, are however hampered by the fact that a large QCD background and the lack of knowledge of the initial centre-of-mass (CM) partonic energies render difficult the task of determining sparticle properties (masses, couplings, quantum numbers, etc.). An insight into this ‘SUSY spectrum’ would in fact shed light on the yet unknown mechanism leading to SUSY-breaking.

In contrast, in e^+e^- collisions, the QCD noise is under control and the initial energies of the leptons are generally well known. This has contributed in the recent years to the generation of a strong consensus behind the option of building electron-positron Linear Colliders (LCs), operating in the energy range from 500 GeV to 3 TeV, as the accelerators most suited to inherit the legacy of the Run II and LHC era [1]. Such machines would not only provide the ideal environment for discovering the SUSY particles which could be missed out at the FNAL and CERN experiments, but would also allow for the precise determination of the mentioned SUSY spectrum. For example, mass measurements are aided by the ability to perform threshold scans by varying the collider CM energy. Furthermore, the spin properties of many SUSY particles can be accessed by exploiting an efficient beam polarisation, a feature altogether missing at the Tevatron and the LHC.

Another advantage of LCs is that they can easily be converted to run quite simply in e^-e^- mode or even in $e\gamma$ and $\gamma\gamma$, the latter by using Compton back-scattering of laser photons against the electrons/positrons [2, 3], all such collisions taking place with energy and luminosity comparable to those obtainable from the primary e^+e^- design. Quite apart from SUSY [4], it should be recalled that electron-electron collisions would constitute a privileged window on, *e.g.*, models with extended Higgs sectors whereas those employing photon beams would easily allow for, *e.g.*, the study of a plethora of QCD topics.

To come back to SUSY, it should be mentioned that there have been in the recent years quite promising explorations of the physics potential of $\gamma\gamma$ LCs as a probe of the low energy dynamics of the theory [5]. It is the intention of our study to further dwell on this topic, by considering the scope of LCs in accessing some R-parity-violating (RPV) signals of SUSY.

2 R-parity-violating Supersymmetry

The construction of the most general Supersymmetric extension of the SM leads to Baryon-(B)- and Lepton-(L)-number-violating operators in the superpotential

$$W_{\mathcal{R}} = \epsilon_i \lambda_{ijk} \hat{L}_i \hat{L}_j \hat{E}_k^c + \lambda'_{ijk} \hat{L}_i \hat{Q}_j \hat{D}_k^c + \epsilon_i \hat{L}_i \hat{H}_2 + \lambda''_{ijk} \hat{U}_i^c \hat{D}_j^c \hat{D}_k^c. \quad (1)$$

Here, \hat{H}_1, \hat{H}_2 are the $SU(2)$ doublets Higgs superfields which give rise to the masses of down-type and up-type quark superfields, respectively, $\hat{L}(\hat{Q})$ denotes lepton(quark) doublet superfields, $\hat{E}^c, \hat{D}^c, \hat{U}^c$ are the singlet lepton and quark superfields, i, j, k are the generational indices and we have suppressed the $SU(2)$ and $SU(3)$ indices. The λ_{ijk} are anti-symmetric in i and j while the λ''_{ijk} are anti-symmetric in j and k . The first three terms in $W_{\mathcal{R}}$ violate lepton number and the last term violates baryon number conservation. The simultaneous presence of both B- and L-violating operators would induce rapid proton decay which would contradict the strict experimental bound of [6]. In order to keep the proton lifetime within the experimental limit, one needs to impose an additional symmetry beyond the SM gauge symmetry, in order to force the unwanted B- and L-violating interactions to vanish. In most cases, this can be achieved by imposing a discrete symmetry, called R-parity [7], defined as $R = (-1)^{3B+L+2S}$, where S is the spin. This symmetry not only forbids rapid proton decay [8] but also renders stable the lightest supersymmetric particle (LSP).

However, R-parity is quite an *ad hoc* assumption in nature, as there are no strong theoretical arguments to support it. Therefore, it is much justified to investigate the phenomenological consequences of RPV SUSY. Extensive studies have been carried out in order to look for direct as well as indirect evidence of trilinear R-parity violation in different processes at various colliders as well as in order to put constraints on various RPV couplings [9].

Resonant sneutrino production in $\gamma\gamma$ collisions has been studied in Ref. [12], where the rare decays into two photons or gluons were considered. In this article, we will consider instead RPV single production of sneutrinos in association with fermion pairs in polarised photon-photon collisions at 500 GeV and 1 TeV LCs, and their subsequent decays into two further fermions, via trilinear L-violating operators, while preserving B-conservation. The latter channel is in our opinion more suited as a sneutrino ‘search’ mode in $\gamma\gamma$ collisions than the former, simply because one can scan a wider range of sneutrino masses $M_{\tilde{\nu}}$ (as long as $\sqrt{s_{\gamma\gamma}} \approx 0.8\sqrt{s_{e^+e^-}} \gg M_{\tilde{\nu}}$), thanks to the fact that some amount of energy is carried away by the accompanying fermion pair, whereas in direct production the only $M_{\tilde{\nu}}$ attainable is basically the (reduced) CM energy itself. Furthermore, the associate mode may also induce flavour changing final states, so that – as pointed out in [13] – unlike in the case of resonant production, one has that the corresponding signatures are basically SM background free. Schematically, one has

$$\gamma\gamma \rightarrow \tilde{\nu} \ell^\pm \ell'^{\mp} \quad \text{or} \quad \tilde{\nu} q \bar{q}' \quad (2)$$

with

$$\tilde{\nu} \rightarrow \ell''^{\pm} \ell'''^{\mp} \quad \text{or} \quad \tilde{\nu} \rightarrow q'' \bar{q}''' , \quad (3)$$

where the ℓ 's refer to e, μ and τ leptons and the q 's to d, u, s, c and b quarks. Finally, the main advantage of exploiting $\gamma\gamma$ collisions in place of e^+e^- ones [10, 11] in producing single sneutrinos in association with a fermion pair in final states of the type (2) resides in the fact that the cross sections for the former are generally larger than those for the latter, as one can appreciate in Figure 1. There, as an illustration, we have plotted the unpolarised production rates for both the $\gamma\gamma$ and e^+e^- induced modes, using the photon structure functions given in [2], at $\sqrt{s_{e^+e^-}} = 500$ GeV and 1 TeV. Apart from the $\tilde{\nu}e^+e^-$ final state, which in electron-positron annihilation receives very large additional contributions from small angle Bhabha-like scattering amplitudes (with respect to the other final states), the photon processes are dominant over the electron-positron ones¹.

The $\gamma\gamma$ induced associate production process has been investigated recently in Ref. [13], by assuming unpolarised photon beams and without any detailed background estimates. We will improve on that study by exploiting polarised $\gamma\gamma$ scatterings, as it has been shown that a high degree of polarisation can be transmitted from the electrons, positrons and laser photons to the Compton back-scattered photons, and by including a study of the irreducible SM background². In fact, it will be shown that polarisation may help to improve the signal-to-background ratio (S/B) in some instances. We consider a general MSSM parameter space, with no assumption on the mechanism of SUSY-breaking, hence defining all parameters at the EW scale.

Before proceeding to the analysis, it is useful to note at this point that the ϵ_i terms in (1) can in principle be removed by a re-definition of the lepton doublets \hat{L}_i , which would in turn lead to their ‘absorption’ into the λ, λ' couplings and in the parameters of the scalar potential of the SUSY model. However, the ϵ_i 's could then re-appear at a different energy scale. Bilinear terms could also lead to a possible vacuum expectation value (VEV) for the sneutrino(s) and mixing of: (a) charged leptons with charginos, (b) sleptons with charged Higgs bosons, (c) neutrinos with neutralinos and (d) sneutrinos with neutral Higgs bosons. This last mixing could indeed affect the process discussed here. However, this phenomenon is suppressed by the small Yukawa couplings of our ℓ and q fermions, so that we feel justified in neglecting it here (*i.e.*, we are making the

¹We will defer the study of the e^+e^- processes to another paper [14]. We should however mention here that we have verified that, given the final luminosities collected at LEP2 (see Ref. [15]), the signatures considered in (2)–(3) but produced via e^+e^- annihilations between 2060 and 210 GeV could have not been seen at the CERN machine, for the choice of RPV couplings adopted in the following (see also [16]).

²We make use of HELAS [17] and MadGraph [18] to produce the helicity amplitudes, for both signal and backgrounds, and integrate these numerically by using VEGAS [19].

assumption that the ϵ_i terms are small)³.

The paper is organised as follows. In section 3, we discuss the phenomenology of processes (2)–(3) in presence of polarised incoming photons. In section 4 we present our numerical results (including those for the backgrounds), followed by our conclusions in section 5.

3 Singly produced sneutrinos at polarised photon colliders

In the RPV MSSM, the sneutrino displays a coupling with pairs of leptons (λ -type couplings) and quarks (λ' -type couplings). Single production of sneutrino in association with fermion pairs in (2) can occur through any of these two types of L-violating couplings. Depending upon the nature of the vertex involved, the above process may also lead to flavour changing final states.

The polarised photon flux and polarisation have been worked out in [2] and are discussed in details in Ref. [3]. For brevity, we do not reproduce here those formulae, rather we simply recall to the un-familiar reader the basic features of polarised $\gamma\gamma$ scatterings.

1. We assume that the laser back-scattering parameter assumes its maximum value, $z \equiv z_{\max} = 2(1 + \sqrt{2}) \simeq 4.828$ [2]. In fact, with increasing z the high energy photon spectrum becomes more mono-chromatic. However, for $z > z_{\max}$, the probability of e^+e^- pair creation increases, resulting in larger photon beam degradation.
2. The reflected photon beam carries off only a fraction x of the e^\pm energy, with $x_{\max} = z/(1+z) \simeq 0.8$, while $x_{\min} = (M_{\tilde{\nu}} + m_f + m_{\bar{f}})/\sqrt{s_{e^+e^-}}$ (hereafter, $f^{(\prime)} = \ell, q$).
3. The polarization of the two initial laser (γ) and electron/positron (e) beams are defined by $P_{\gamma-}, P_{\gamma+}, P_{e-}$ and P_{e+} , respectively, where, for the first two quantities, $-(+)$ identifies the laser colliding against the electron(positron).
4. Finally, one can cast the polarised production cross-section in the following form:

$$\begin{aligned} \sigma_{e^+e^- \rightarrow \gamma\gamma \rightarrow \tilde{\nu} f \bar{f}'}(s) = & \int dx_- dx_+ F_-^{\gamma/e}(P_{e-}, P_{\gamma-}, x_-; P_-) F_+^{\gamma/e}(P_{e+}, P_{\gamma+}, x_+; P_+) \\ & \times \hat{\sigma}_{\gamma\gamma \rightarrow \tilde{\nu} f \bar{f}'}(\hat{s}, P_-, P_+), \end{aligned} \quad (4)$$

where $x_{-(+)}$ is the electron(positron) momentum fraction carried by the emerging photon, $x_- x_+ = \hat{s}_{\gamma\gamma}/s_{e^+e^-}$, with $s_{e^+e^-}(\hat{s}_{\gamma\gamma})$ being the CM energy squared of the $e^+e^-(\gamma\gamma)$ system,

³This would not be possible for processes involving top (anti)quarks, because of their large mass. However, in (2)–(3), t quarks contributions will have negligible impact, because strongly suppressed by phase space effects. (Some phenomenological consequences of a sneutrino VEV and L-violating mixing have been discussed in literature [20].)

and $F_{\pm}^{\gamma/e}(P_{e\pm}, P_{\gamma\pm}, x_{\pm}; P_{\pm})$ the photon distribution functions, defined in terms of $P_{e\pm}, P_{\gamma\pm}$ and x_{\pm} and yielding $P_{-}(P_{+})$, the degree of polarisation of the photon that has back-scattered against the electron(positron)⁴. Therefore, in terms of helicity amplitudes one has (here, for brevity, $\hat{\sigma} \equiv \hat{\sigma}_{\gamma\gamma \rightarrow \bar{\nu} f \bar{f}'}$)

$$\begin{aligned} \hat{\sigma}(\hat{s}, P_{-}, P_{+}) = & \frac{1}{4} [(1 + P_{-})(1 + P_{+})\hat{\sigma}_{++}(\hat{s}) + (1 + P_{-})(1 - P_{+})\hat{\sigma}_{+-}(\hat{s}) \\ & + (1 - P_{-})(1 + P_{+})\hat{\sigma}_{-+}(\hat{s}) + (1 - P_{-})(1 - P_{+})\hat{\sigma}_{--}(\hat{s})]. \end{aligned} \quad (5)$$

As polarised γ -structure functions we have used those of Ref. [21].

The flavour of the final state fermions will depend upon the RPV couplings involved. It has been shown that most of the first two generation L-violating terms are highly constrained from different low and medium energy processes [22]. For our study, we made the assumption that just one L-violating coupling at a time is the dominant one, so that only bounds derived under the same hypothesis are relevant. This restriction may seem unnatural, however, it is a useful approach that allows one to derive a quantitative feeling for the phenomenological consequences of RPV interactions, while avoiding a proliferation of SUSY input parameters. In our analysis, we will concentrate on the following L-violating couplings: $\lambda_{311}, \lambda_{323}, \lambda'_{323}$ and λ'_{333} . The reason for selecting this particular set out of the 36 possible couplings is that these are less constrained and at the same time can lead to a significant contribution to the production as well as the decay rates of sneutrinos in (2)–(3). The upper limits on these couplings and the processes which give such bounds are shown in Table 1. Notice that all these limits scale as $M_{\tilde{f}}/100$ GeV with the common

Coupling	Upper Limit	Sources
λ_{311}	0.062	$R_{\tau} = \frac{\Gamma(\tau \rightarrow e\nu\bar{\nu})}{\Gamma(\tau \rightarrow e\mu\bar{\nu})}$ [11]
λ_{323}	0.070	"
λ'_{323}	0.52	$R_{D_s} = \frac{\Gamma(D_s \rightarrow \tau\nu_{\tau})}{\Gamma(D_s \rightarrow \mu\nu_{\mu})}$ [23]
λ'_{333}	0.45	"

Table 1: Experimental (2σ) upper bounds on the RPV couplings relevant to this analysis. All sfermion masses are assumed to be 100 GeV.

sfermion mass. That is, they become weaker as $M_{\tilde{f}}$ increases. However, some couplings are constrained by the requirement of perturbative unitarity. For example, the corresponding bound on λ'_{323} is 1.12. Indeed, we could have taken any values of these couplings bounded between the mentioned upper and lower limits (as done by [12]). However, like in [13] and for the sake of

⁴Conventionally, one has $P_{-(+)} = -1(+1)$ for purely left(right) handed photons.

simplicity, we will consider only one fixed value for each of the RPV couplings, the one obtained assuming a 100 GeV sfermion mass (as in Table 1). In a sense then, our approach can be viewed as conservative.

Once the sneutrino is produced, it will decay. Depending on its nature, the dominant decay modes are:

$$\tilde{\nu} \rightarrow f\bar{f}' \quad (f = \ell, q) \quad \text{fermion pairs}, \quad (6)$$

$$\tilde{\nu} \rightarrow \tilde{\chi}_i^0 \nu \quad (i = 1, 2, 3, 4) \quad \text{neutralino} + \text{neutrino}, \quad (7)$$

$$\tilde{\nu} \rightarrow \tilde{\chi}_i^+ \ell^- \quad (i = 1, 2) \quad \text{chargino} + \text{lepton}. \quad (8)$$

If the sneutrino is the LSP, then it will decay through the first (RPV) channel, otherwise via one of the other two (MSSM) modes. We show the sneutrino branching ratio (BR) into two fermion final states in the $\mu - M_2$ plane for a fixed value of $\tan\beta$, RPV coupling and sneutrino mass. In the course of the analysis we assume the Grand Unification (GUT) relationship between the $U(1)$ and $SU(2)$ gaugino mass parameters: *i.e.*,

$$M_1 = \frac{5}{3} \tan^2 \theta_W M_2. \quad (9)$$

Hence, the sneutrino BR into two fermions will depend upon μ , M_2 , $\tan\beta$, $M_{\tilde{\nu}}$ and the magnitude of the RPV coupling. To study the variation of the sneutrino RPV BR we have spanned μ from -500 GeV to $+500$ GeV and M_2 from 100 GeV to 500 GeV.

In Figure 2(a) we show the contours of constant $\text{BR}(\tilde{\nu}_\tau \rightarrow e^+e^-)$ through the λ_{311} coupling for $M_{\tilde{\nu}_\tau} = 100$ GeV in the $\mu - M_2$ plane, with $\tan\beta = 5$. The region labelled by ‘LEP DISALLOWED’ is ruled out from the kinematic limit on the lighter chargino mass extracted from LEP-2 data. It can be seen from this Figure that the mentioned BR is 90% over a large part of the parameter space. In this case, the lighter chargino is heavier than the sneutrino mass, forbidding the $\tilde{\nu} \rightarrow \tilde{\chi}_1^+ \ell^-$ decay channel. The only MSSM channel allowed is $\tilde{\nu} \rightarrow \tilde{\chi}_1^0 \nu$, which dominates in the low M_2 region, where $M_{\tilde{\chi}_1^0} < M_{\tilde{\nu}}$. The above scenario changes once the sneutrino becomes heavier, as shown in Figure 2(b), where the same BR as above is plotted but now with $M_{\tilde{\nu}} = 200$ GeV. In this case, both channels $\tilde{\nu} \rightarrow \tilde{\chi}_1^+ \ell^-$ and $\tilde{\nu} \rightarrow \tilde{\chi}_1^0 \nu$ make a significant contribution to the total decay width of the sneutrino. (The RPV BR increases with M_2 though, since the lighter chargino and neutralino become heavier.) In Figure 2(c), this trend becomes very clear: for a 400 GeV sneutrino most of the $\mu - M_2$ plane is covered by the MSSM decays, relegating large RPV BRs to small corners of the parameter space.

This situation changes considerably when the RPV coupling is λ'_{333} . In this case, because of the larger magnitude of the latter, as compared to λ_{311} , the $\text{BR}(\tilde{\nu} \rightarrow b\bar{b})$ for a 100 GeV sneutrino mass covers almost the entire $\mu - M_2$ plane analysed in this paper. Even for heavier sneutrinos (*e.g.*, 200 GeV and 400 GeV), a larger area in the $\mu - M_2$ plane is dominated by the above BR,

leaving a smaller region for the MSSM decays than in the previous case: see Figures 2(d)–(f). Finally, we have noticed that this general behavior of the BRs does not change for higher values of $\tan\beta$. Also, the impact of λ_{323} and λ'_{323} RPV couplings onto the decay rates induces a pattern similar to the one discussed, so we do not reproduce the corresponding Figures here.

4 Numerical analysis

We perform our numerical analysis for three different points in the MSSM parameter space allowed by LEP-2 data. These are representative of three different natures of the lightest chargino and are defined in Table 2.

Set	μ (GeV)	M_2 (GeV)	$\tan\beta$	$M_{\tilde{\chi}_1^0}$ (GeV)	$M_{\tilde{\chi}_1^\pm}$ (GeV)	Nature of $\tilde{\chi}_1^\pm$
A	−400	150	5	76.4	150.3	Gaugino dominated state
B	200	350	40	150.4	185.6	Mixed state
C	175	500	40	155.6	169.4	Higgsino dominated state

Table 2: Set of selected points in the MSSM parameter space with LSP and lighter chargino mass (and nature) given explicitly (we defer to the Appendix the listing of the total decay widths of the sneutrino in different RPV channels for these three choices of MSSM parameters).

Furthermore, we select the combinations of incident laser and electron beam polarisations shown in Table 3.

	$P_{\gamma+}$	$P_{\gamma-}$	P_{e+}	P_{e-}
$\sigma(+ -)$	+1	−1	−0.8	+0.9
$\sigma(+ +)$	+1	+1	−0.8	−0.9
$\sigma(00)$	0	0	0	0

Table 3: Values of laser and electron(positron) beam polarisations adopted in our analysis. The $\sigma(+ -)$ and $\sigma(+ +)$ denote the corresponding polarised production cross-sections, with $\sigma(00)$ the unpolarised one.

The choice $P_{\gamma_\pm} P_{e_\pm} < 0$ guarantees not only good mono-chromaticity, but also a high degree of circular polarisation of the produced photons as compared to the case $P_{\gamma_\pm} P_{e_\pm} > 0$. There exists a symmetry amongst the four combinations of laser polarizations, as $(+ -)$ and $(- +)$ give

the same result, and so do $(++)$ and $(--)$ (see also [21]).

To mimic the finite coverage of the LC detectors, we impose the following cuts on the final state particles in (2)⁵:

$$5^\circ < \theta < 175^\circ \quad (\text{angular cut on both leptons and jets}), \quad (10)$$

$$E_\ell > 5 \text{ GeV} \quad (\text{energy cut on leptons}), \quad (11)$$

$$E_j > 10 \text{ GeV} \quad (\text{energy cut on jets}). \quad (12)$$

As already mentioned, we assume that only one between the λ and λ' couplings dominates at a time. Besides, we will treat the signatures arising from the four RPV couplings considered here, *i.e.*, λ_{311} , λ_{323} , λ'_{323} and λ'_{333} , separately in the four subsections below. Where appropriate, all possible electromagnetic (EM) charge combinations (c.c.'s) will be included. Moreover, we assume that the EM charge of the leptons (e , μ and τ) can always be determined, unlike the case of quarks. For the latter, we will assume a benchmark 100% efficiency in tagging b flavours.

4.1 Signals from the λ_{311} coupling

Presence of this coupling leads $\tilde{\nu}_\tau$ to decay into e^+e^- pairs. Hence, the signal corresponding to this L-violating coupling is $e^+e^-e^+e^-$. In Figure 3(a) we show the variation of $\sigma(\gamma\gamma \rightarrow \tilde{\nu}_\tau e^+e^-) * \text{BR}(\tilde{\nu}_\tau \rightarrow e^+e^-)$ as a function of the $\tilde{\nu}_\tau$ mass for the MSSM set A, at $\sqrt{s_{e^+e^-}} = 500 \text{ GeV}$. The effect of beam polarisation can be seen very clearly from the figure. At very low sneutrino masses ($< 150\text{--}200 \text{ GeV}$), $\sigma(++)$, $\sigma(+-)$ and the unpolarised cross-section $\sigma(00)$ are basically the same. As the sneutrino mass rises, the above three cross-section display a hierarchy, though not dramatic, with $\sigma(+-) > \sigma(00) > \sigma(++)$, whereas, for $M_{\tilde{\nu}_\tau} \geq 0.5\sqrt{s_{e^+e^-}}$, the $\sigma(++)$ component is the one which largely dominates. A similar situation can be seen for the other two sets of MSSM parameters, namely sets B and C, in Figures 4(a) and 5(a), respectively. For $\sqrt{s_{e^+e^-}} = 1 \text{ TeV}$, corresponding plots are given in Figures 6(a), 7(a) and 8(a), for the MSSM parameter sets A, B and C, respectively. At higher energies, the pattern is very similar, with the only exceptions that in this case $\sigma(00)$ is slightly larger than the other two at small sneutrino masses and the mentioned hierarchy onsets for somewhat larger values of the latter, in comparison to the lower energy collider option.

4.2 Signals from the λ_{323} coupling

Presence of this coupling gives rise to the following two types of signals: flavour conserving $\tau^+\tau^-\tau^+\tau^-$ and flavour changing $\mu^+\mu^-\tau^+\tau^-$ (and c.c.'s). The variation of $\sigma(\gamma\gamma \rightarrow \tilde{\nu}_\tau \mu^+\tau^-) *$

⁵We identify jets with the partons from which they originate.

$\text{BR}(\tilde{\nu}_\tau \rightarrow \mu^- \tau^+)$ as a function of the sneutrino mass is shown in Figures 3(b) 4(b) and 5(b), for $\sqrt{s_{e^+e^-}} = 500$ GeV, and Figures 6(b), 7(b) and 8(b) for $\sqrt{s_{e^+e^-}} = 1$ TeV, corresponding to the MSSM parameter sets A, B and C, respectively. In this case the final state will have three different combinations of charged particles with identical rates: $\mu^+ \mu^- \tau^+ \tau^-$, $\mu^+ \mu^+ \tau^- \tau^-$ and $\mu^- \mu^- \tau^+ \tau^+$. Hence, the individual channels will be 1/3 of the total cross-section shown in the Figures. The plots for the flavour conserving final states are displayed in Figures 3(c), 4(c) and 5(c), for $\sqrt{s_{e^+e^-}} = 500$ GeV, and Figures 6(c), 7(c) and 8(c), for $\sqrt{s_{e^+e^-}} = 1$ TeV.

In this case too we see that the dominant cross-section comes from $\sigma(++)$ once the $M_{\tilde{\nu}_\tau} \geq 0.5\sqrt{s_{e^+e^-}}$. However, at lower sneutrino masses, the pattern is different from the previous case. The ordering $\sigma(+-) > \sigma(00) > \sigma(++)$ in the intermediate mass regime and the convergence of the rates for all polarisation states at small $M_{\tilde{\nu}_\tau}$ values hold only for $\tau^+ \tau^- \tau^+ \tau^-$, not for $\mu^+ \mu^- \tau^+ \tau^-$ (plus c.c.s), for which the unpolarised cross sections are always largest. In this case, again, the increase in CM energy delays the onset of the highlighted cross section hierarchy, for $\tau^+ \tau^- \tau^+ \tau^-$ final states.

4.3 Signals from the λ'_{323} coupling

Presence of this coupling gives rise to the following three types of signals: the flavour conserving $s\bar{s}s\bar{s}$ and $b\bar{b}b\bar{b}$ plus the flavour changing $s\bar{s}b\bar{b}$ (and c.c.'s). The variation of $\sigma(\gamma\gamma \rightarrow \tilde{\nu}_\tau b\bar{s}) * \text{BR}(\tilde{\nu}_\tau \rightarrow \bar{b}s)$ as a function of the sneutrino mass is shown in Figures 3(e), 4(e) and 5(e), for $\sqrt{s_{e^+e^-}} = 500$ GeV, and Figures 6(e), 7(e) and 8(e) for $\sqrt{s_{e^+e^-}} = 1$ TeV, again, in correspondence of the MSSM parameter sets A, B and C, respectively. Notice that in this case too there are three equiprobable signatures: $s\bar{s}b\bar{b}$, $s\bar{s}b\bar{b}$ and $\bar{s}sbb$. Corresponding plots for the flavour conserving modes are displayed in Figures 3(d), 4(d) and 5(d), for $\sqrt{s_{e^+e^-}} = 500$ GeV, and Figures 6(d), 7(d) and 8(d) for $\sqrt{s_{e^+e^-}} = 1$ TeV (in correspondence of sets A,B and C).

The dependence upon the beam polarisation configuration is basically the same as the one described in the previous section, once one establishes a correspondence between the identical- and different-flavour final states in the two cases. The energy dependence does not differ much either from that in the two previous cases.

4.4 Signals from the λ'_{333} coupling

Presence of this coupling will also give rise to the signal $b\bar{b}b\bar{b}$. The numerical results for the corresponding production cross-sections are shown in Figures 3(f), 4(f) and 5(f), for $\sqrt{s_{e^+e^-}} = 500$ GeV, and Figures 6(f), 7(f) and 8(f) for $\sqrt{s_{e^+e^-}} = 1$ TeV, corresponding to the MSSM parameter sets A, B and C, respectively.

As for the beam polarisation dependence, here, one can see the usual dominance of $\sigma(++)$

whenever $M_{\tilde{\nu}_\tau} \geq 0.5\sqrt{s_{e^+e^-}}$, with the $\sigma(+ -)$ component dominating in the intermediate regime. For lower masses, the energy dependence is such that at 500 GeV $\sigma(+ -)$ is above $\sigma(00)$, whereas at 1 TeV things go the other way around.

4.5 Signals from $\tilde{\nu} \rightarrow \tilde{\chi}_1^+ \ell^-$

Here, we would like to comment about the signal cross-section $\sigma(\gamma\gamma \rightarrow \tilde{\nu} f \bar{f}) * \text{BR}(\tilde{\nu} \rightarrow \tilde{\chi}_1^+ \ell^-)$ for two different RPV interactions, namely λ_{311} and λ'_{323} . Figures 10(a)–(c) correspond to $\sigma(\gamma\gamma \rightarrow \tilde{\nu}_\tau e^+ e^-) * \text{BR}(\tilde{\nu}_\tau \rightarrow \tilde{\chi}_1^+ \tau^-)$ for $\lambda_{311} = 0.062$ whereas the variation of $\sigma(\gamma\gamma \rightarrow \tilde{\nu} s \bar{b}) * \text{BR}(\tilde{\nu}_\tau \rightarrow \tilde{\chi}_1^+ \tau^-)$ with the sneutrino mass (for $\lambda'_{323} = 0.52$) is shown in Figures 10(d)–(f). Notice that Figures 10(a,d), 10(b,e) and 10(c,f) correspond to the three usual sets of MSSM parameters A, B and C, respectively. These cross-sections have been calculated for the case of a LC of 500 GeV. The pattern of the production and decay rates is here quite different from the one displayed for the case of RPV decays of the sneutrino. In fact, the overall behaviour in this channel depends on other factors. Firstly, on the relative mass difference between $\tilde{\nu}$ and $\tilde{\chi}_1^+$, as well as upon the composition of $\tilde{\chi}_1^+$ (if it is Higgsino dominated, then the $\tilde{\nu} - \tilde{\chi}_1^+ - \ell^-$ coupling will be Yukawa suppressed). Secondly, and most importantly, the magnitude of the RPV coupling involved: as it is clear from comparing Figures 10(a)–(c) to Figure 10(d)–(f), the stronger the RPV coupling the smaller the $\tilde{\nu} \rightarrow \tilde{\chi}_1^+ \ell^-$ decay mode. In other words, this signal is somehow complementary to the RPV ones discussed so far and requires a different discussion of the decay dynamics, given the additional dependence on the chargino mass. Hence, although this signature may well induce visible events in the end, we do not pursue further its study here.

4.6 The SM irreducible background

If $M_{\tilde{\nu}}$ is very near the EW scale, say, 80–90 GeV, it is clear that the dominant SM irreducible background to RPV signals of the type discussed in the previous sections arises from associated production of a Z boson and a fermionic pair, with the gauge boson decaying into two further fermions:

$$\gamma\gamma \rightarrow Z \ell^\pm \ell^\mp \quad \text{or} \quad Z q \bar{q} \quad (13)$$

with

$$Z \rightarrow \ell'^\pm \ell'^\mp \quad \text{or} \quad Z \rightarrow q' \bar{q}'. \quad (14)$$

Only in the case of four-quark final states one has to deal with W^\pm mediated production:

$$\gamma\gamma \rightarrow W^\pm q \bar{q}' \quad (15)$$

with

$$W^\pm \rightarrow q'' \bar{q}''' \quad (16)$$

	$e^+e^-e^+e^-$	$\mu^+\mu^-\tau^+\tau^-*$	$\tau^+\tau^-\tau^+\tau^-$	$s\bar{s}s\bar{s}$	$s\bar{s}b\bar{b}^*$	$b\bar{b}b\bar{b}$
$\sigma(+ -)$	4.7×10^9	2169	232	532048	3409	313
$\sigma(+ +)$	4.7×10^9	2288	233	551620	3485	317
$\sigma(00)$	4.7×10^9	2228	232	541824	3447	315
$\sqrt{s_{e^+e^-}} = 500 \text{ GeV}$						
$\sigma(+ -)$	1.9×10^9	1054	114	241093	1629	161
$\sigma(+ +)$	1.9×10^9	1042	115	240166	1707	162
$\sigma(00)$	1.9×10^9	1048	114	240612	1668	161
$\sqrt{s_{e^+e^-}} = 1 \text{ TeV}$						
*Other c.c.'s are free from SM background						

Table 4: Cross sections in femtobarns for the full four-fermion SM processes discussed in the text, for the three beam polarisation configurations in Table 3, after the cuts in (10) (and $M_{e^+e^-} > 1$ GeV for the $e^+e^-e^+e^-$ final state). Notice that no summation over u, d and s (light) flavours has been performed in the case of signatures involving s quarks.

However, notice that, with the exception of the $s\bar{s}s\bar{s}$ signature, only Cabibbo-Kobayashi-Maskawa (CKM) suppressed channels can contribute in (15)–(16), if one assumes a fully efficient heavy quark tagging (via a displaced vertex) to be available at future LCs (*i.e.*, $\epsilon_{c,b} = 100\%$). This is precisely what occurs in the case of $s\bar{s}b\bar{b}$ final states whereas W^\pm mediated SM backgrounds cannot contribute to $b\bar{b}b\bar{b}$ final states under the above assumption (we will briefly discuss the more realistic scenario arising from a finite efficiency for the latter in the last section).

When the sneutrino mass starts departing from M_Z (or M_W), then a variety of SM subprocesses could produce sizable irreducible backgrounds, although at very heavy $M_{\tilde{\nu}}$ values only the tails of the SM distributions can actually play a role. All these channels can be conveniently grouped into general four-fermion final states, of the type $e^+e^-e^+e^-$, $\mu^+\mu^-\tau^+\tau^-$, $\tau^+\tau^-\tau^+\tau^-$, $s\bar{s}s\bar{s}$, $s\bar{s}b\bar{b}$ and $b\bar{b}b\bar{b}$, which we have generated by means of all Feynman graphs appearing at leading order, with the only exclusion of Higgs mediated graphs, which are irrelevant for the first four channels, because of the smallness of the Yukawa couplings involved (see also footnote 6), and since they can easily be excluded in the last two cases via a suitable invariant mass cut, *i.e.*, $M_{b\bar{b}} \neq M_{\text{Higgs}}$, for any known neutral Higgs mass state of the model, thanks to the narrowness of the Higgs boson resonances below the $W^\pm W^\mp$ threshold.

The first three signatures only receive EW contributions (*i.e.*, they are of $\mathcal{O}(\alpha^4)$), whereas the last three also have a QCD induced component of $\mathcal{O}(\alpha^2\alpha_s^2)$. Under the assumption of perfect b

$M_{\tilde{\nu}}$ (GeV)	$e^+e^-e^+e^-$	$\mu^+\mu^-\tau^+\tau^-^*$	$\tau^+\tau^-\tau^+\tau^-$	$s\bar{s}s\bar{s}$	$s\bar{s}b\bar{b}^*$	$b\bar{b}b\bar{b}$
100	0.1908	0.4650	0.2565	2.387	2.100	1.3091
	1.1865	1.4177	1.3095	2.4466	2.1270	1.3529
	1.1865	1.4177	1.3095	2.4466	2.1270	1.3529
	382042836	56	19	93366	627	63
200	0.00234	0.00695	0.00313	0.3870	0.4019	0.17967
	0.03256	0.08342	0.04208	0.5939	0.51151	0.30668
	0.6004	0.13705	0.07569	0.6055	0.51651	0.31462
	93921298	6.4	4.4	22248	170	18
300	0.000171	0.000493	0.000222	0.04387	0.0477	0.01649
	0.00112	0.003163	0.001461	0.09135	0.07628	0.03892
	0.00267	0.007204	0.003431	0.10293	0.08134	0.04533
	19052146	3.6	1.7	3696	30	3.3
*Other c.c.'s are free from SM background						

Table 5: Cross sections in femtobarns for the four-fermion final states discussed in the text, for both signals (first three rows for MSSM set A,B and C respectively) and backgrounds (last row), for unpolarised beams at $\sqrt{s_{e^+e^-}} = 500$ GeV, after the cuts in (10) plus the additional constraint $|M_{ff} - M_{\tilde{\nu}}| < 5$ GeV, for several sneutrino masses. (Here, ff refer to either lepton-lepton or jet-jet pairs and only one $M_{\tilde{\nu}}$ is required to be reconstructed.) Notice that, for the backgrounds, no summation over u, d and s (light) flavours has been performed in the case of signatures involving s quarks.

(and c) quark tagging, we only need to sum over light quark flavours in the case of $s\bar{s}s\bar{s}$ and $s\bar{s}b\bar{b}$ final states, not of $b\bar{b}b\bar{b}$. However, in order to save computing time, we have presently refrained from doing so, as the EW and QCD contributions involving only s (anti)quarks, as opposed to the sum over u, d and s , already swamp the signal in the accessible $M_{\tilde{\nu}}$ regions. (All forthcoming $s\bar{s}s\bar{s}$ and $s\bar{s}b\bar{b}$ background rates will then be reported for s flavours only.)⁶ Of course, four-fermion final states computed this way also include the contributions of processes of the type (13)–(14) and (15)–(16).

The SM background cross-sections, after the cuts listed in eq. (10), are given in Table 4. A

⁶Also, we have used the two-loop expression for α_s , as a function of the energy scale $Q \equiv \sqrt{s_{\gamma\gamma}}$ and of $\Lambda_{\text{QCD}}^{n_f=4} = 0.230$ GeV.

$M_{\tilde{\nu}}$ (GeV)	$e^+e^-e^+e^-$	$\mu^+\mu^-\tau^+\tau^-*$	$\tau^+\tau^-\tau^+\tau^-$	$s\bar{s}s\bar{s}$	$s\bar{s}b\bar{b}^*$	$b\bar{b}b\bar{b}$
100	0.1313	0.3268	0.1860	1.7951	1.6455	1.0897
	0.8168	0.9963	0.9496	1.8394	1.6659	1.1262
	0.8168	0.9963	0.9496	1.8394	1.6659	1.1262
	206634870	48	14	39993	271	28
200	0.00269	0.00801	0.00401	0.4869	0.5385	0.2621
	0.03740	0.09613	0.05383	0.7471	0.6854	0.4474
	0.06897	0.1579	0.09681	0.7617	0.6921	0.4590
	59351446	8.0	8.2	15451	163	16
300	0.000486	0.001532	0.000701	0.1459	0.1913	0.07331
	0.003192	0.009818	0.004616	0.3039	0.3059	0.1729
	0.007567	0.02235	0.01083	0.3424	0.3262	0.2014
	23373961	3.7	1.1	7005	47	7.3
400	0.000189	0.0005867	0.000282	0.06167	0.08462	0.03029
	0.000997	0.003023	0.001452	0.1351	0.1432	0.07438
	0.002332	0.006881	0.003376	0.1610	0.1579	0.09261
	11211595	2.3	0.93	2393	19	2.3
500	8.476×10^{-5}	0.0002556	0.000117	0.02832	0.03792	0.01336
	0.000226	0.000685	0.000320	0.05041	0.05710	0.02544
	0.000920	0.002706	0.001305	0.07713	0.07362	0.04249
	5294773	0.38	0.22	1335	8	1.0
*Other c.c.'s are free from SM background						

Table 6: Same as Table 5 for $\sqrt{s}_{e^+e^-} = 1$ TeV.

common feature to all rates is that they are basically independent of the polarisation state of the initial particles⁷. By comparing the background rates in Table 4 to those for the signals in Figures 3–8, it is clear that the former are overwhelming the latter in the *inclusive* cross sections. However, several selection cuts can be applied in order to improve the signal-to-background ratio (S/B). For example, the Z mediated noise in four-lepton final states can be reduced by requiring

⁷The huge rates for the $e^+e^-e^+e^-$ final state should not be surprising: on the one hand, because of the t, u channel soft and collinear singularities of the total cross section (which are only regulated by the small electron mass); on the other hand, since we have implemented rather loose constraints in order to avoid these, *i.e.*, other than the cuts in individual energy and polar angles of eq. (10) we only required $M_{e^+e^-} > 1$ GeV on all electron-positron pairs (this combination is sufficient to obtain a numerically stable answer).

$M_{\tilde{\nu}}$ (GeV)	$e^+e^-e^+e^-$	$\mu^+\mu^-\tau^+\tau^-$	$\tau^+\tau^-\tau^+\tau^-$	$s\bar{s}s\bar{s}$	$s\bar{s}b\bar{b}$	$b\bar{b}b\bar{b}$
100	0.00031	2.0	1.9	0.25	2.7	5.2
	0.0019	6.0	9.5	0.25	2.7	5.4
	0.0019	6.0	9.5	0.25	2.7	5.4
200	7.6×10^{-6}	0.087	0.047	0.082	0.97	1.3
	0.00011	1.0	0.63	0.13	1.2	2.3
	0.0020	1.7	1.14	0.13	1.3	2.3
300	1.2×10^{-6}	0.0082	0.0054	0.023	0.28	0.29
	8.1×10^{-6}	0.053	0.035	0.048	0.44	0.68
	1.9×10^{-5}	0.12	0.083	0.054	0.47	0.79

Table 7: Significances S/\sqrt{B} at $\sqrt{s_{e^+e^-}} = 500$ GeV after 1 ab^{-1} for the four-fermion final states discussed in the text, for both signals (first three rows for MSSM set A,B and C respectively) and backgrounds (last row), for unpolarised beams, after the cuts in (10) plus the additional constraint $|M_{ff} - M_{\tilde{\nu}}| < 5$ GeV, for several sneutrino masses. (Here, ff refer to either lepton-lepton or jet-jet pairs and only one $M_{\tilde{\nu}}$ is required to be reconstructed.) Notice that, for the backgrounds, no summation over u, d and s (light) flavours has been performed in the case of signatures involving s quarks.

that no $\ell^+\ell^-$ pairs of opposite charge (with $\ell = e, \mu$) reproduces the Z mass within a few GeV (say, 3 or 4 GeV, given the good mass resolution expected at LCs for electrons and muons). Similarly, one can proceed for four-quark final states, by rejecting events with one (or more) jet-jet invariant masses in the vicinity of the Z and W^\pm peaks. The 4τ signature is more difficult to deal with in this respect, because of the missing momentum carried away by the neutrinos. Finally, QCD induced four-jet backgrounds tend to produce at least one jet-jet pair with small invariant mass.

In the very end, however, one should keep in mind that we are dealing with sneutrino masses that are bound by current experimental constraints to be above the EW scale. Hence, in general, by restricting oneself to the most interesting mass range, sufficiently far from the Z and W^\pm masses, say, 100–150 GeV or above, the chances of extracting the RPV signals in some of the channels discussed become evident, if one refers to Figure 9 and to the rates in Figures 3–8.

By finally recalling that sneutrinos yield mass resonances that are rather narrow (see the typical widths in the Appendix), one can further enhance the S/B by restricting the candidate sample around the resonances. To this end, we present Table 5 and 6, where, alongside the signal

$M_{\tilde{\nu}}$ (GeV)	$e^+e^-e^+e^-$	$\mu^+\mu^-\tau^+\tau^-$	$\tau^+\tau^-\tau^+\tau^-$	$s\bar{s}s\bar{s}$	$s\bar{s}b\bar{b}$	$b\bar{b}b\bar{b}$
100	0.00029	1.5	1.6	0.28	3.1	6.5
	0.0018	4.5	8.0	0.29	3.2	6.7
	0.00179685869	4.54746653	8.0	0.29	3.2	6.7
200	1.1×10^{-5}	0.090	0.044	0.12	1.3	2.1
	0.00015	1.1	0.59	0.19	1.7	3.5
	0.00028	1.8	1.1	0.19	1.7	3.6
300	3.2×10^{-6}	0.025	0.021	0.055	0.88	0.86
	2.1×10^{-5}	0.16	0.14	0.11	1.4	2.0
	4.9×10^{-5}	0.37	0.33	0.13	1.5	2.4
400	1.8×10^{-6}	0.012	0.0092	0.039	0.61	0.63
	9.4×10^{-6}	0.063	0.048	0.087	1.04	1.6
	2.2×10^{-5}	0.14	0.11	0.10	1.1	1.9
500	1.2×10^{-6}	0.013	0.0079	0.025	0.42	0.42
	3.1×10^{-6}	0.035	0.022	0.044	0.64	0.80
	1.3×10^{-5}	0.14	0.088	0.067	0.82	1.3

Table 8: Same as Table 7 for $\sqrt{s}_{e^+e^-} = 1$ TeV.

yield, the surviving background rates are given, after we have required that only one (di-lepton or di-jet) invariant mass reconstructs the resonant sneutrino mass within 10 GeV. Notice that we have accounted for all combinatorics in both leptonic and hadronic final states, assuming EM charge recognition in the former but not in the latter. Results are given for the unpolarised case, for the sake of illustration. (In the case of polarised initial states, the pattern is very similar.)

At the end of this selection, one should expect the final states $\mu^+\mu^-\tau^+\tau^-$, $\tau^+\tau^-\tau^+\tau^-$ and $b\bar{b}b\bar{b}$ to achieve a significance $\sigma \equiv S/\sqrt{B}$ larger than 5 after 1 ab^{-1} of luminosity in the region $M_{\tilde{\nu}} \sim 100\text{--}150$ GeV, at both $\sqrt{s}_{e^+e^-} = 500$ GeV and 1 TeV, for all MSSM parameter sets considered in the case of the hadronic signature and limitedly to set B and C for the leptonic ones. The overall signal rates at that luminosity are about 1,000 events per channel. At the higher collider energy option, an evidence (*i.e.*, $\sigma \gtrsim 3$) of the $4b$ signal may appear also in the $M_{\tilde{\nu}} \sim 200\text{--}250$ GeV interval, at least for the MSSM sets B and C, with overall signal rates of order 500 events. All other signatures appear instead hopeless. Tables (7)–(8) summarise our findings in this respect. The typical signal would then be an excess of $\mu^+\mu^-\tau^+\tau^-$, $\tau^+\tau^-\tau^+\tau^-$ plus $b\bar{b}b\bar{b}$ events above the SM expectations for the corresponding four-fermion processes, with the bulk of the events cantered in a rather narrow lepton-lepton or jet-jet mass region corresponding to the sneutrino mass.

5 Conclusions

Although a full Monte Carlo simulation, including all signals and backgrounds that we have discussed and in presence of both hadronisation and detector effects, should eventually be performed in order to put on firmer ground the results presented here, it is clear that the latter seem rather promising at present.

In practice, if RPV couplings of the type λ_{311} , λ_{323} , λ'_{323} or λ'_{333} are close to their current exclusion bounds, over sizable regions of the MSSM parameter space (particularly, for positive μ values), several four-fermion signatures induced by a sneutrino, with a mass $M_{\tilde{\nu}} \lesssim 150$ GeV if $\sqrt{s_{e^+e^-}} = 500$ GeV and $\lesssim 250$ GeV if $\sqrt{s_{e^+e^-}} = 1$ TeV, produced in association with a fermion pair and decaying itself into a second pair, can be accessed, with the photons produced via back-scattering against the primary electrons and positrons. The typical annual rate should be of several hundreds to a thousand events in each of the three channels $\mu^+\mu^-\tau^+\tau^-$, $\tau^+\tau^-\tau^+\tau^-$ and $b\bar{b}b\bar{b}$, depending on the actual sneutrino mass and assuming a luminosity of 1 ab^{-1} .

Furthermore, since typical SM backgrounds have been seen to be less sensitive than the signals to the polarisation state of the incoming particles, one may exploit the latter in order to improve the discovery potential of RPV signals at future LCs. If a high, but not unrealistic, degree of polarisation of both laser photons and leptonic beams can be achieved, this can be exploited to push the discovery reach in sneutrino mass somewhat beyond the mentioned $M_{\tilde{\nu}}$ values in the $\tau^+\tau^-\tau^+\tau^-$ and $b\bar{b}b\bar{b}$ final states (*i.e.*, those most massive in the leptonic and hadronic case, respectively) at 500 GeV. In fact, at this energy, the polarisation combination in which the electron and positron helicities have the opposite sign and are also opposite to those of the corresponding laser photons, *i.e.*, $(+-)$, yields, for sneutrino masses in the 100–250 GeV region, signal rates somewhat higher than those induced in the other cases (including that of unpolarised beams), up to a factor of 2. In contrast, for the $\mu^+\mu^-\tau^+\tau^-$ final state, it is the unpolarised configuration, *i.e.*, (00) , the most suitable for sneutrino searches in the above mass range. Once the collider energy is raised to 1 TeV, differences between the three polarisation combinations almost disappear if $M_{\tilde{\nu}} \lesssim 250$ GeV. The polarisation state in which the electron and positron helicities have the same sign and opposite to the one of the laser photons, *i.e.*, $(++)$, would turn out extremely useful for heaviest sneutrino masses, say, when $M_{\tilde{\nu}} \gtrsim \sqrt{s_{e^+e^-}}/2$, as here signal rates are consistently and significantly above those induced by the other polarisations, up to a factor of 4 in some instances. Unfortunately, this mass interval is unattainable through present LC designs (TESLA, NLC and JLC) and will have to attend for higher collider energies, such as those foreseen for CLIC ($\sqrt{s_{e^+e^-}} \gtrsim 3$ TeV).

Before closing, two final considerations are in order. Firstly, recall that, as a bonus of the production process considered here, some leptonic signatures which are flavour changing, such as $\mu^+\mu^+\tau^-\tau^-$ and $\mu^-\mu^-\tau^+\tau^+$, would come practically free from SM background, hence promptly

detectable at a future LC. Secondly, that we have not included the effect of finite experimental efficiency in tagging leptons and jets, so that our final significances may be somewhat overestimated. The comment particularly applies to the $4b$ final state, for which we have assumed throughout a 100% efficiency for a quadruple b -tagging. If one adopts a more realistic 70% per b -jet, significances in the last columns in Tables (7)–(8) would go down by a factor of 2, hampering seriously the scope of the hadronic channel. However, one may alternatively consider to tag only a subset of the four b -quarks. The correct estimate of the potential in this channel clearly depends on the tagging strategy of b -quarks and can only be obtained in the context of a fully hadronic environment and in presence of detector effects, which were lacking in our study. However, in the worse case scenario in which the $b\bar{b}b\bar{b}$ signature of RPV sneutrinos produced in associated mode is swamped by the backgrounds, one should still be able to resort to $\mu^+\mu^-\tau^+\tau^-$ and $\tau^+\tau^-\tau^+\tau^-$. Altogether, we consider the subject raised in this paper of relevance for the physics of future LCs and look forward to experimental studies in the context of the current LC workshops.

6 Acknowledgements

We thank Abdesselam Arhrib for discussions. The work of DKG is supported by the National Science Council of Taiwan under the grant NSC 90-2811-M-002-054 and from the Ministry of Education Academic Excellence Project 89-N-FA01-1-4-3 of Taiwan.

7 Appendix

As intimated in the main text, we reproduce here the sneutrino partial widths in the two-body decay channels considered in the paper, see Table 9, for the MSSM parameter sets given in Table 2.

$M_{\tilde{\nu}}$ (GeV)	e^+e^-	$\mu^+\tau^-$	$\tau^+\tau^-$	$s\bar{s}$	$s\bar{b}$	$b\bar{b}$
100	0.0238	0.0297	0.0248	0.8269	1.6270	0.6169
200	0.6474	0.6593	0.6495	2.2536	3.8640	1.8447
400	4.1109	4.1345	4.1151	7.3232	10.5492	6.5109

$M_{\tilde{\nu}}$ (GeV)	e^+e^-	$\mu^+\tau^-$	$\tau^+\tau^-$	$s\bar{s}$	$s\bar{b}$	$b\bar{b}$
100	0.0038	0.0097	0.0049	0.8069	1.6070	0.5970
200	0.0642	0.0760	0.0663	1.6704	3.2808	1.2614
400	0.8613	0.8850	0.8655	4.0737	7.2996	3.2613

$M_{\tilde{\nu}}$ (GeV)	e^+e^-	$\mu^+\tau^-$	$\tau^+\tau^-$	$s\bar{s}$	$s\bar{b}$	$b\bar{b}$
100	0.0038	0.0097	0.0049	0.8069	1.6070	0.5970
200	0.0294	0.0413	0.0315	1.6356	3.2460	1.2267
400	0.3975	0.4212	0.4017	3.6099	6.8359	2.7976

Table 9: Sneutrino decay width (in GeV) in the RPV decay channels relevant to our analysis for the MSSM parameter sets A (top), B (middle) and C (bottom).

References

- [1] K. Abe *et al.*, [The ACFA Linear Collider Working Group], hep-ph/0109166 and references therein; T. Abe *et al.*, [The American Linear Collider Working Group], hep-ex/0106055; hep-ex/0106056; hep-ex/0106057 and hep-ex/0106058 and references therein; J.A. Aguilar-Saavedra *et al.*, [The ECFA/DESY LC Physics Working Group], preprint SLAC-REPRINT-2001-002, DESY-01-011, DESY-2001-011, DESY-01-011C, DESY-2001-011C, DESY-TESLA-2001-23, DESY-TESLA-FEL-2001-05, ECFA-2001-209, March 2001, hep-ph/0106315; G. Guignard (editor), [The CLIC Study Team], preprint CERN-2000-008.
- [2] I. Ginzburg, G. Kotkin, V. Serbo and V. Telnov, *Nucl. Instrum. Meth. A* **205**, 47 (1983); *ibidem* **A 219**, 5 (1984); V. Telnov, *Nucl. Instrum. Meth. A* **294**, 72 (1990).
- [3] V. Telnov, hep-ex/0010033 and references therein.
- [4] F. Cuyppers, G.J. van Oldenborgh and R. Ruckl, *Nucl. Phys.* **B409**, 144 (1993).
- [5] S. Berge, M. Klasen and Y. Umeda, *Phys. Rev. D* **63**, 35003 (2001); A. Datta and D. Choudhury, *Nucl. Phys.* **B592**, 35 (2001); T. Mayer and H. Fraas, *Nucl. Instrum. Meth. A* **472**, 165 (2001); D. Gorbunov, V. Ilyin and V. Telnov, *Nucl. Instrum. Meth. A* **472**, 171 (2001); D.M. Asner, J.B. Gronberg and J.F. Gunion, hep-ph/0110320 and references therein.
- [6] D. E. Groom *et al.*, [Particle Data Group], *Eur. Phys. J.* **C15**, 1 (2000).
- [7] P. Fayet, *Phys. Lett.* **B69**, 489 (1977); G. Farrar and P. Fayet, *Phys. Lett.* **B76**, 575 (1978); N. Sakai and T. Yanagida, *Nucl. Phys.* **B197**, 533 (1982); C. Aulakh and R. Mohapatra, *Phys. Lett.* **B119**, 136 (1983).
- [8] S. Weinberg, *Phys. Rev. D* **26**, 287 (1982).
- [9] L.J. Hall and M. Suzuki, *Nucl. Phys.* **B231**, 419 (1984); R. Barbieri and A. Masiero, *Nucl. Phys.* **B267**, 679 (1986); S. Dimopoulos and L.J. Hall, *Phys. Lett.* **B207**, 210 (1988); V. Barger, G. F. Giudice and T. Han, *Phys. Rev. D* **40**, 2987 (1989); M. Czakon and J. Gluza, hep-ph/0003228; R. Godbole, P. Roy and X. Tata, *Nucl. Phys.* **B401**, 67 (1993); G. Bhattacharyya, J.R. Ellis and K. Sridhar, *Mod. Phys. Lett.* **A10**, 1583 (1995); G. Bhattacharyya, D. Choudhury and K. Sridhar, *Phys. Lett.* **B355**, 193 (1995); D. Choudhury and S. Raychaudhury, *Phys. Lett.* **B401**, 54 (1997); D.K. Ghosh, S. Raychaudhuri and K. Sridhar, *Phys. Lett.* **B396**, 177 (1997); K. Huitu, J. Maalampi, M. Raidal and A. Santamaria, *Phys. Lett.* **B430**, 355 (1998); G. Moreau, ‘*Phenomenological study of the interactions violating the R-parity symmetry in the supersymmetric theories*’, Ph.D. Thesis, hep-ph/0012156 and references therein.

- [10] S. Dimopoulos and L.J. Hall, in [9]; M. Czakon and J. Gluza, in [9].
- [11] V. Barger, G. F. Giudice and T. Han, in [9].
- [12] S. Bar-Shalom, G. Eilam, J. Wudka and A. Soni, *Phys. Rev. D* **59**, 035010 (1999).
- [13] M. Chaichian, K. Huitu, S. Roy and Z.H. Yu, *Phys. Lett.* **B518**, 261 (2001).
- [14] D.K. Ghosh and S. Moretti, in preparation.
- [15] K. Jacobs, preprint UMZ-01-0720, July 2001, hep-ex/0107084; see also:
<http://sl.web.cern.ch/SL/opnews/pageswww/lcnov2000/sld005.htm>.
- [16] D. Abbaneo *et al.*, [ALEPH Collaboration], preprint CERN-EP/2001-094, January 2002, hep-ex/0201013.
- [17] H. Murayama, I. Watanabe and K. Hagiwara, HELAS: HELicity Amplitude Subroutines for Feynman Diagram Evaluations, *KEK Report* 91–11, January 1992.
- [18] T. Stelzer and W.F. Long, *Comp. Phys. Comm.* **81**, 357 (1994).
- [19] G.P. Lepage, *Jour. Comp. Phys.* **27**, 192 (1978).
- [20] L.J. Hall and M. Suzuki in Ref. [9]; I-H. Lee, *Phys. Lett.* **B138**, 121 (1984); *Nucl. Phys.* **B246**, 120 (1984); S. Dawson, *Nucl. Phys.* **B261**, 297 (1985); F. de Campos, M.A. Garcia-Jareno, A.S. Joshipura, J. Rosiek and J.W.F. Valle, *Nucl. Phys.* **B451**, 3 (1995); M. Nowakowski and A. Pilaftsis, *Nucl. Phys.* **B461**, 19 (1996); R. Hempfling, *Nucl. Phys.* **B478**, 3 (1996); S. Roy and B. Mukhopadhyaya, *Phys. Rev. D* **55**, 7020 (1997); M. Hirsch, M.A. Díaz, W. Porod, J.C. Romao and J.W.F. Valle, *Phys. Rev. D* **62**, 3008 (2000).
- [21] S. Berge, M. Klasen and Y. Umeda, in Ref. [5].
- [22] See, *e.g.*: B.C. Allanach, A. Dedes and H.K. Dreiner, *Phys. Rev. D* **60**, 075014 (1999) and references therein.
- [23] F. Ledroit and G. Sajot, note GDR-S-008 (ISN, Grenoble, 1998), see:
http://qcd.th.u-psud.fr/GDR_SUSY/GDR_SUSY_PUBLIC/entete_note_publique.

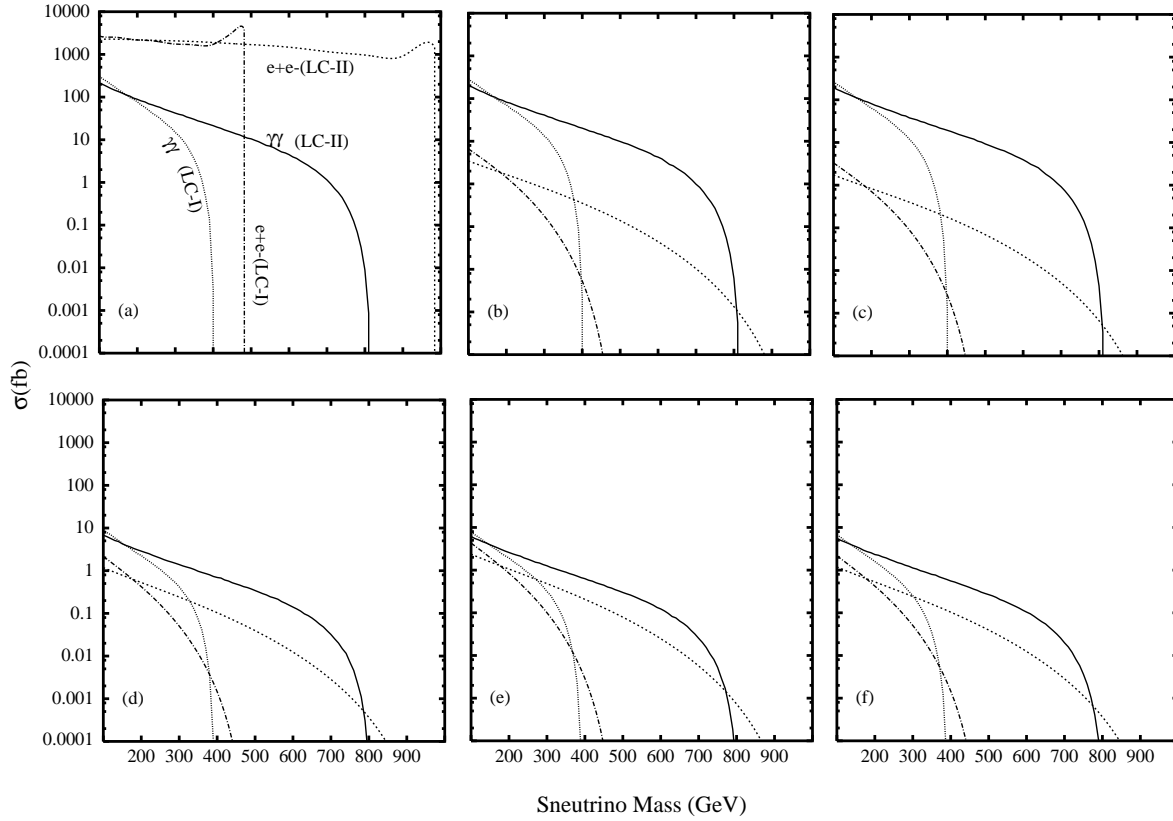


Figure 1: Cross sections for following production processes : $\tilde{\nu}e^+e^-$ (a), $\tilde{\nu}\tau^+\mu^- + (c.c.)$ (b), $\tilde{\nu}\tau^+\tau^-$ (c), $\tilde{\nu}s\bar{s}$ (d), $\tilde{\nu}b\bar{b} + (c.c.)$ (d), $\tilde{\nu}b\bar{b}$ (f), at $\gamma\gamma$ collider (solid) and their in e^+e^- annihilation (dashed), as a function of the sneutrino mass $M_{\tilde{\nu}}$, at $\sqrt{s_{e^+e^-}} = 500$ GeV (LC-I) and 1 TeV (LC-II), after the cuts in (10). For simplicity, we have set the parity violating couplings λ and λ' to 1.

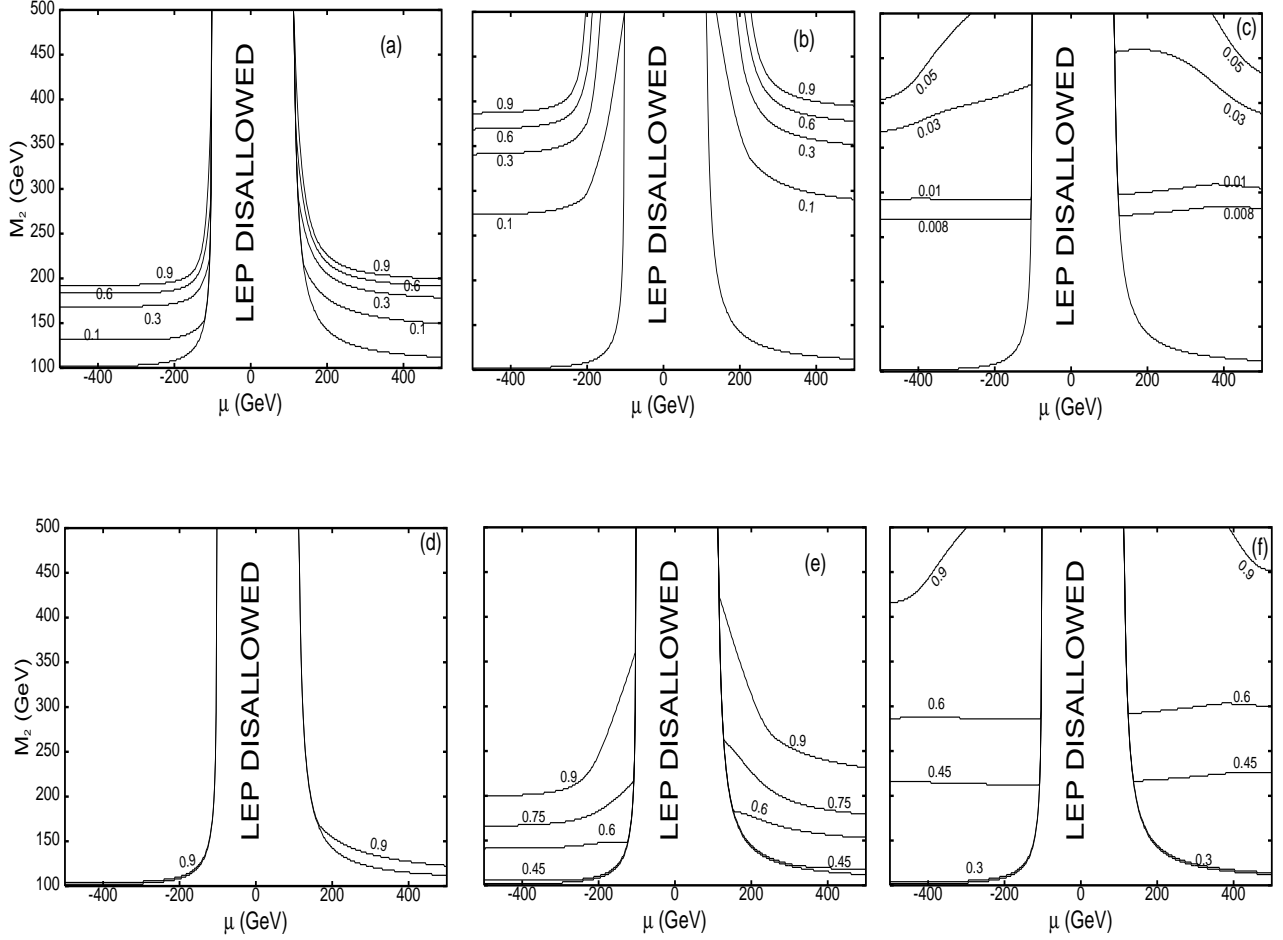


Figure 2: Constant BR contours of the decay $\tilde{\nu}_\tau \rightarrow e^+e^-$ for three values of sneutrino masses: 100 GeV (a), 200 GeV (b) and 400 GeV (c). Figures (d)–(f) represents contours of constant BR($\tilde{\nu}_\tau \rightarrow b\bar{b}$), again for a 100, 200 and 400 GeV sneutrino mass, respectively. The relevant L-violating couplings are here: $\lambda_{311} = 0.062$ for (a)–(c) and $\lambda'_{333} = 0.45$ for (d)–(f). The level curves are function of μ and M_2 , whereas the other relevant MSSM parameters are those of set A in Table. 2 below.

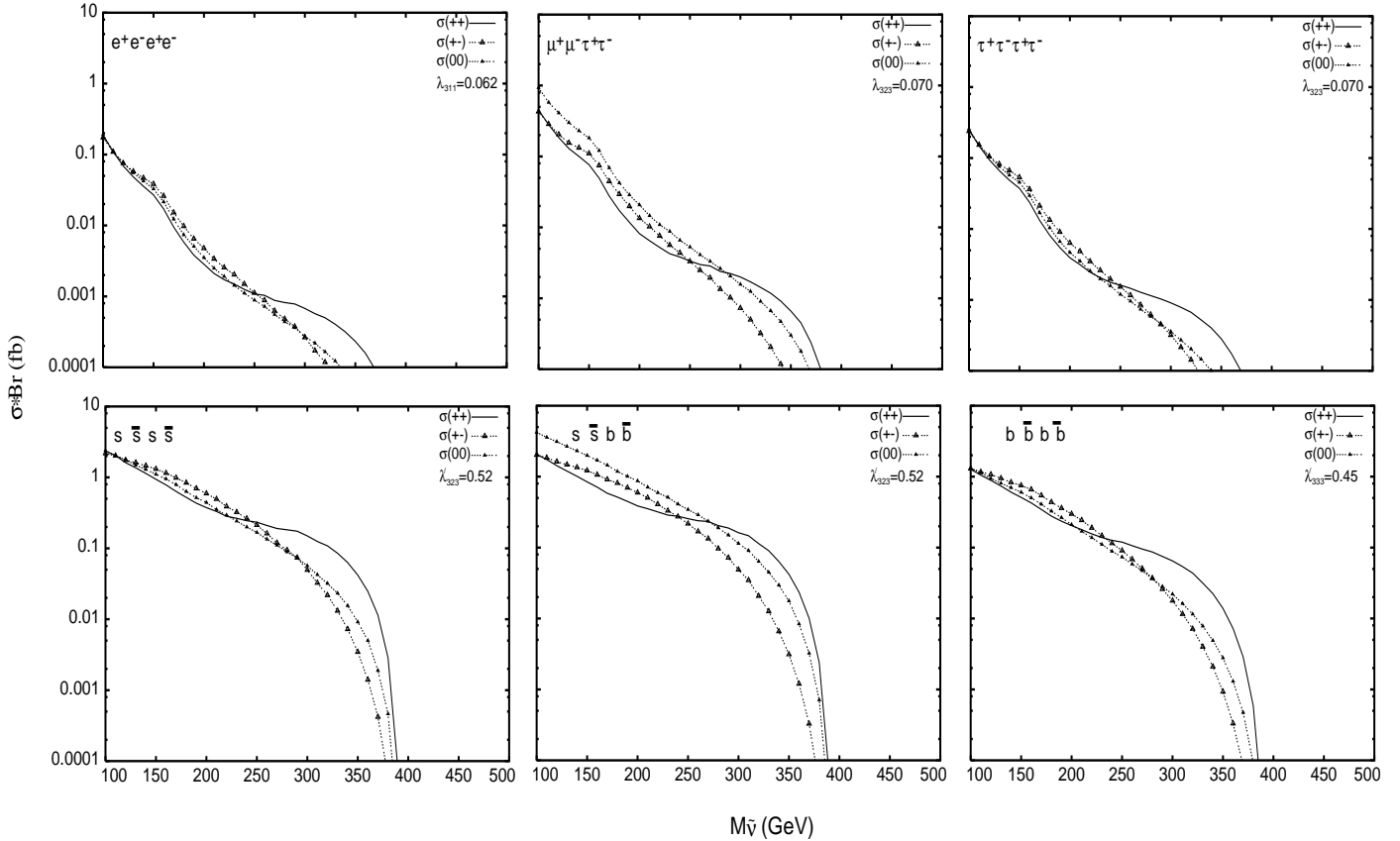


Figure 3: Variation of $\sigma(\gamma\gamma \rightarrow \tilde{\nu}_i f_j \bar{f}_k) * \text{BR}(\tilde{\nu}_i \rightarrow f_j \bar{f}_k)$ at $\sqrt{s_{e^+e^-}} = 500$ GeV with the sneutrino mass, for fixed values of the relevant λ_{ijk} and λ'_{ijk} couplings. The MSSM parameters are $\mu = -400$ GeV, $M_2 = 150$ GeV and $\tan \beta = 5$ (set A). Final state fermions are shown in the respective figures. For dissimilar fermions in the final state we include all charge conjugate states. See Table 3 for the definition of (un)polarised cross-sections.

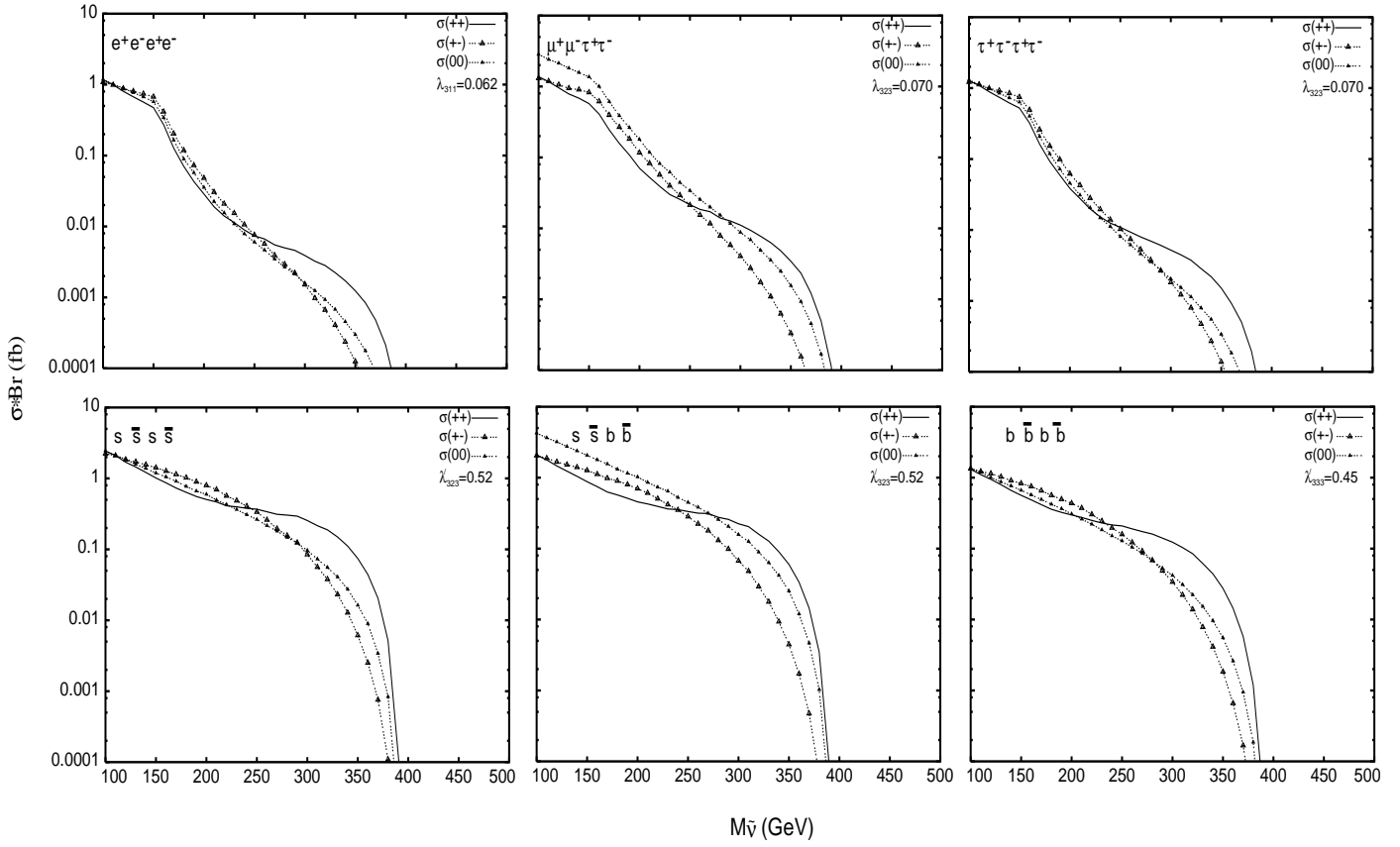


Figure 4: Variation of $\sigma(\gamma\gamma \rightarrow \tilde{\nu}_i f_j \bar{f}_k) * \text{BR}(\tilde{\nu}_i \rightarrow f_j \bar{f}_k)$ at $\sqrt{s_{e^+e^-}} = 500$ GeV with the sneutrino mass, for fixed values of the relevant λ_{ijk} and λ'_{ijk} couplings. The MSSM parameters are $\mu = 200$ GeV, $M_2 = 350$ GeV and $\tan\beta = 40$ (set B). Final state flavours are shown in the each figure. We include the C.C. states for the dissimilar final states.

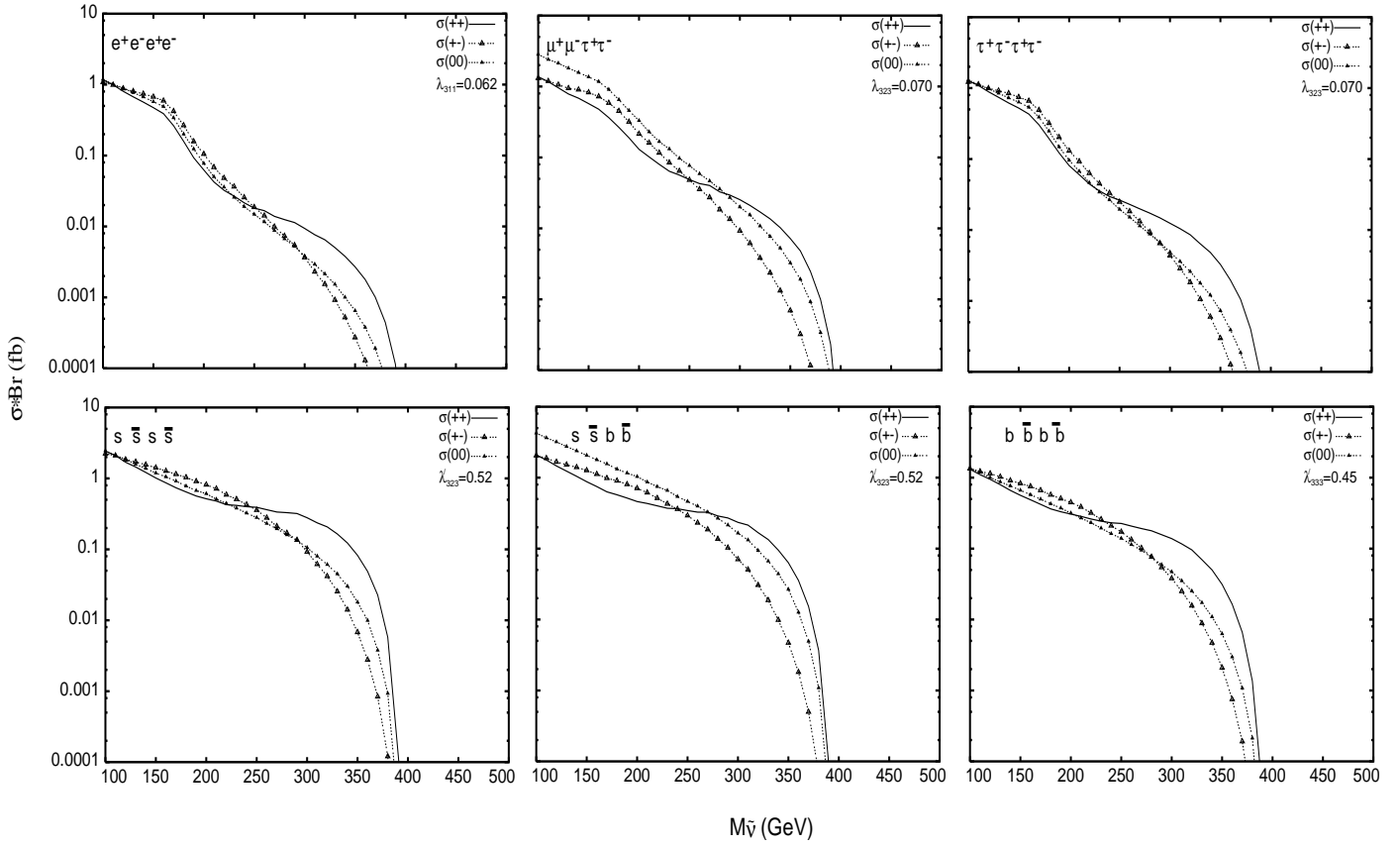


Figure 5: Variation of $\sigma(\gamma\gamma \rightarrow \tilde{\nu}_i f_j \bar{f}_k) * \text{BR}(\tilde{\nu}_i \rightarrow f_j \bar{f}_k)$ at $\sqrt{s_{e^+e^-}} = 500$ GeV with the sneutrino mass, for fixed values of the relevant λ_{ijk} and λ'_{ijk} couplings. The MSSM parameters are $\mu = 175$ GeV, $M_2 = 500$ GeV and $\tan\beta = 40$ (set C). Final state flavours are shown in the each figure. We include the C.C. states for the dissimilar final states.

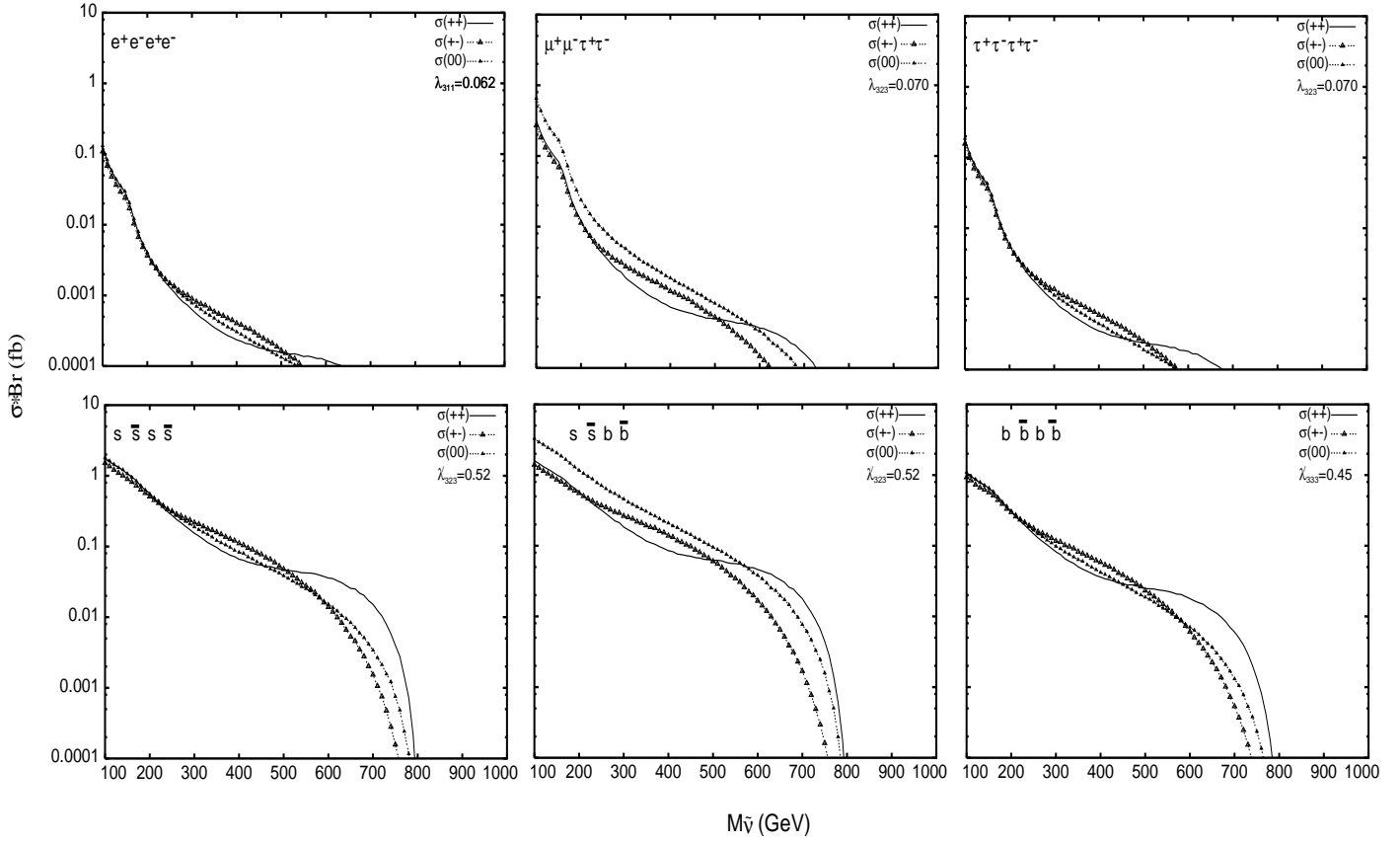


Figure 6: Variation of $\sigma(\gamma\gamma \rightarrow \tilde{\nu}_i f_j \bar{f}_k) * \text{BR}(\tilde{\nu}_i \rightarrow f_j \bar{f}_k)$ at $\sqrt{s_{e^+e^-}} = 1$ TeV with the sneutrino mass, for fixed values of the relevant λ_{ijk} and λ'_{ijk} couplings. The MSSM parameters are $\mu = -400$ GeV, $M_2 = 150$ GeV and $\tan\beta = 5$ (set A). Final state flavours are shown in the each figure. We include the C.C. states for the dissimilar final states.

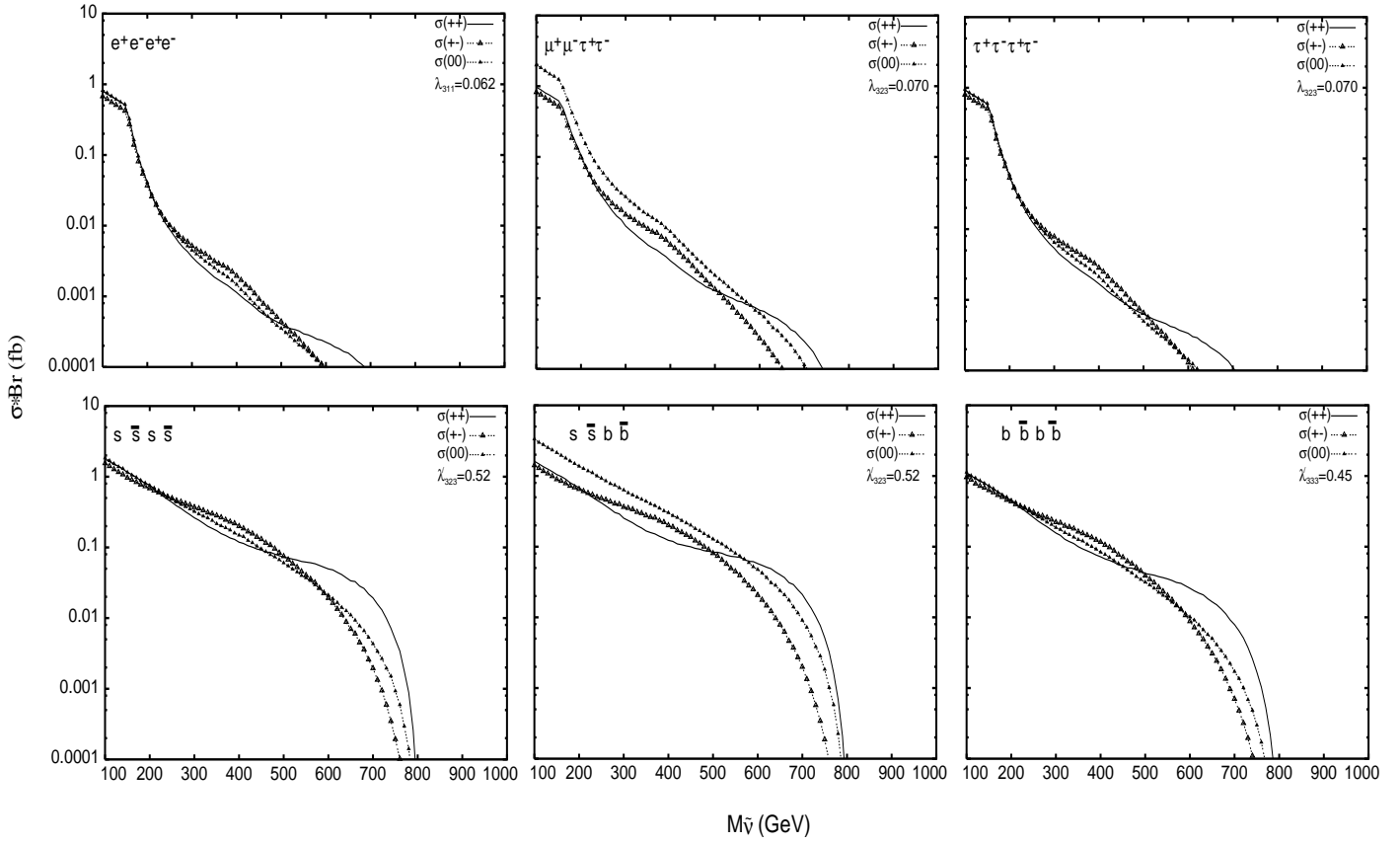


Figure 7: Variation of $\sigma(\gamma\gamma \rightarrow \tilde{\nu}_i f_j \bar{f}_k) * \text{BR}(\tilde{\nu}_i \rightarrow f_j \bar{f}_k)$ at $\sqrt{s_{e^+e^-}} = 1$ TeV with the sneutrino mass, for fixed values of the relevant λ_{ijk} and λ'_{ijk} couplings. The MSSM parameters are $\mu = 200$ GeV, $M_2 = 350$ GeV and $\tan\beta = 40$ (set B). Final state flavours are shown in the each figure. We include the C.C. states for the dissimilar final states.

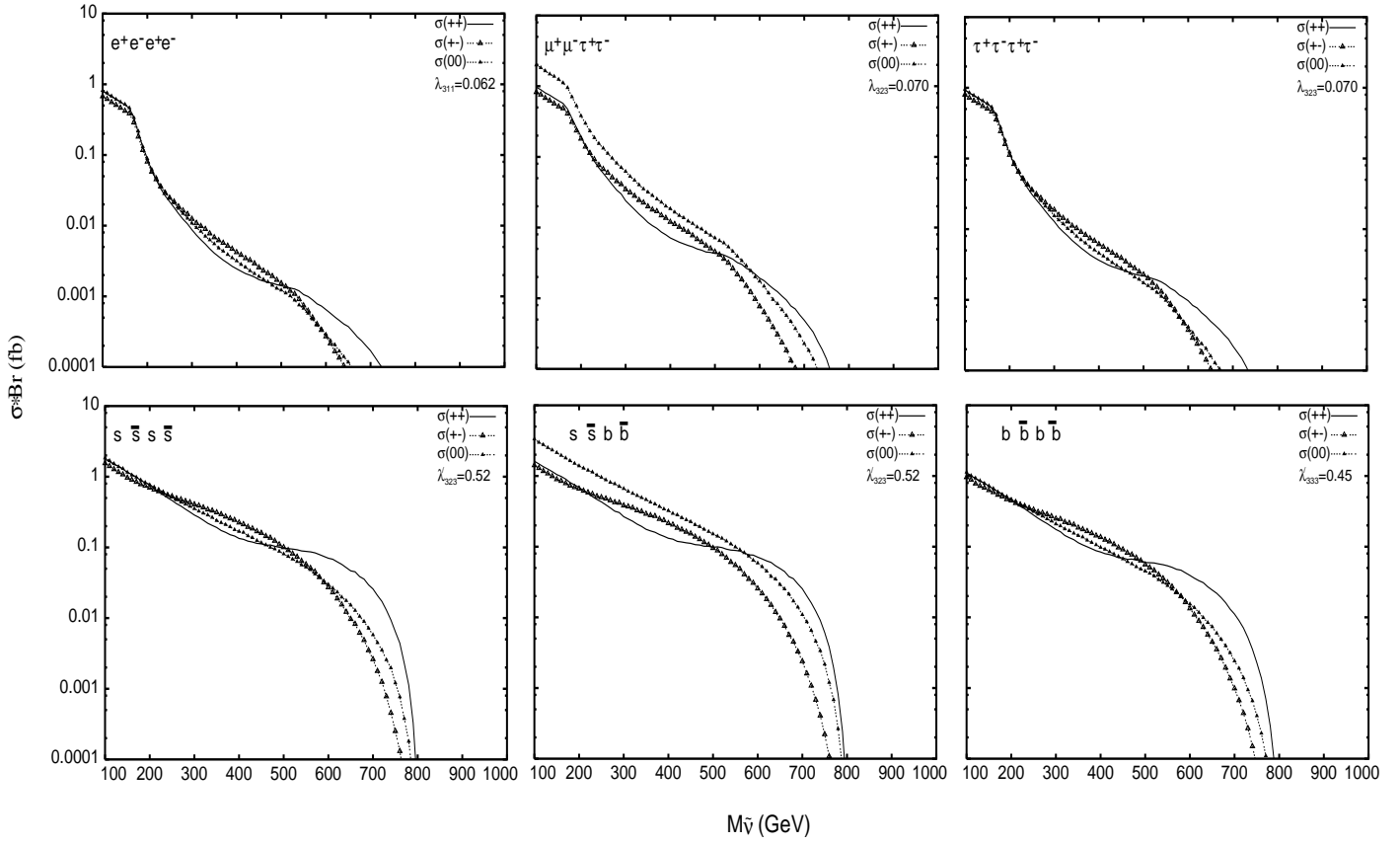


Figure 8: Variation of $\sigma(\gamma\gamma \rightarrow \tilde{\nu}_i f_j \bar{f}_k) * \text{BR}(\tilde{\nu}_i \rightarrow f_j \bar{f}_k)$ at $\sqrt{s_{e^+e^-}} = 1$ TeV with the sneutrino mass, for fixed values of the relevant λ_{ijk} and λ'_{ijk} couplings. The MSSM parameters are $\mu = 175$ GeV, $M_2 = 500$ GeV and $\tan\beta = 40$ (set C). Final state flavours are shown in the each figure. We include the C.C. states for the dissimilar final states.

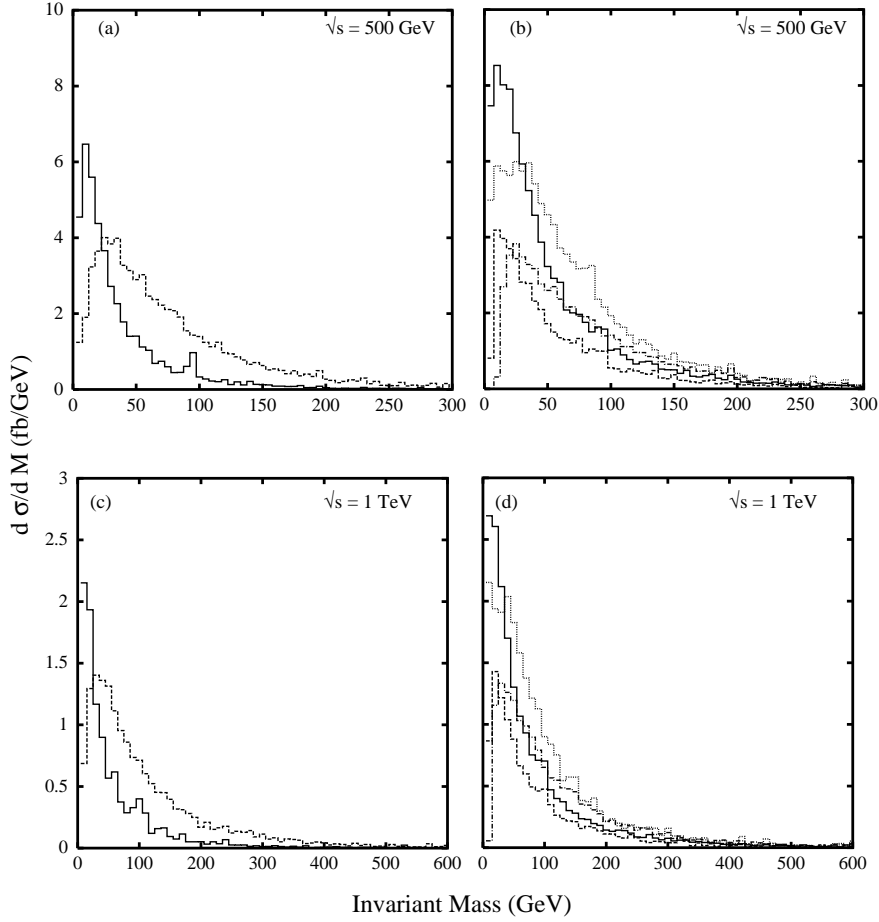


Figure 9: Invariant mass distributions in lepton-lepton and jet-jet pairs reproducing the sneutrino mass in the background processes discussed in the text, for the case of unpolarised beams, $\sqrt{s_{e^+e^-}} = 500$ GeV and 1 TeV, after the cuts in (10) (the additional constraint $M_{e^+e^-} > 1$ GeV has been implemented for the $e^+e^-e^+e^-$ signature, for all possible pairings with opposite EM charge). Normalisation is to the corresponding total cross sections given in Table 4. All possible combinatorial combinations have been plotted, each with the same probability, given by the event weight divided by the number of possible pairings in each case. Bins are 10 GeV wide. Scaling factors have to be applied, in order to obtain the original cross sections, as follows: (a,c) $\mu^+\mu^-\tau^+\tau^-$ (solid) to be scaled by 10^{-2} , $s\bar{s}b\bar{b}$ (dashed) by 10^{-2} ; (b,d) $e^+e^-e^+e^-$ (solid) to be scaled by 10^4 , $\tau^+\tau^-\tau^+\tau^-$ (dashed) by 10^{-3} , $s\bar{s}s\bar{s}$ (dotted) no scaling, $b\bar{b}b\bar{b}$ (dot-dashed) by 10^{-3} .

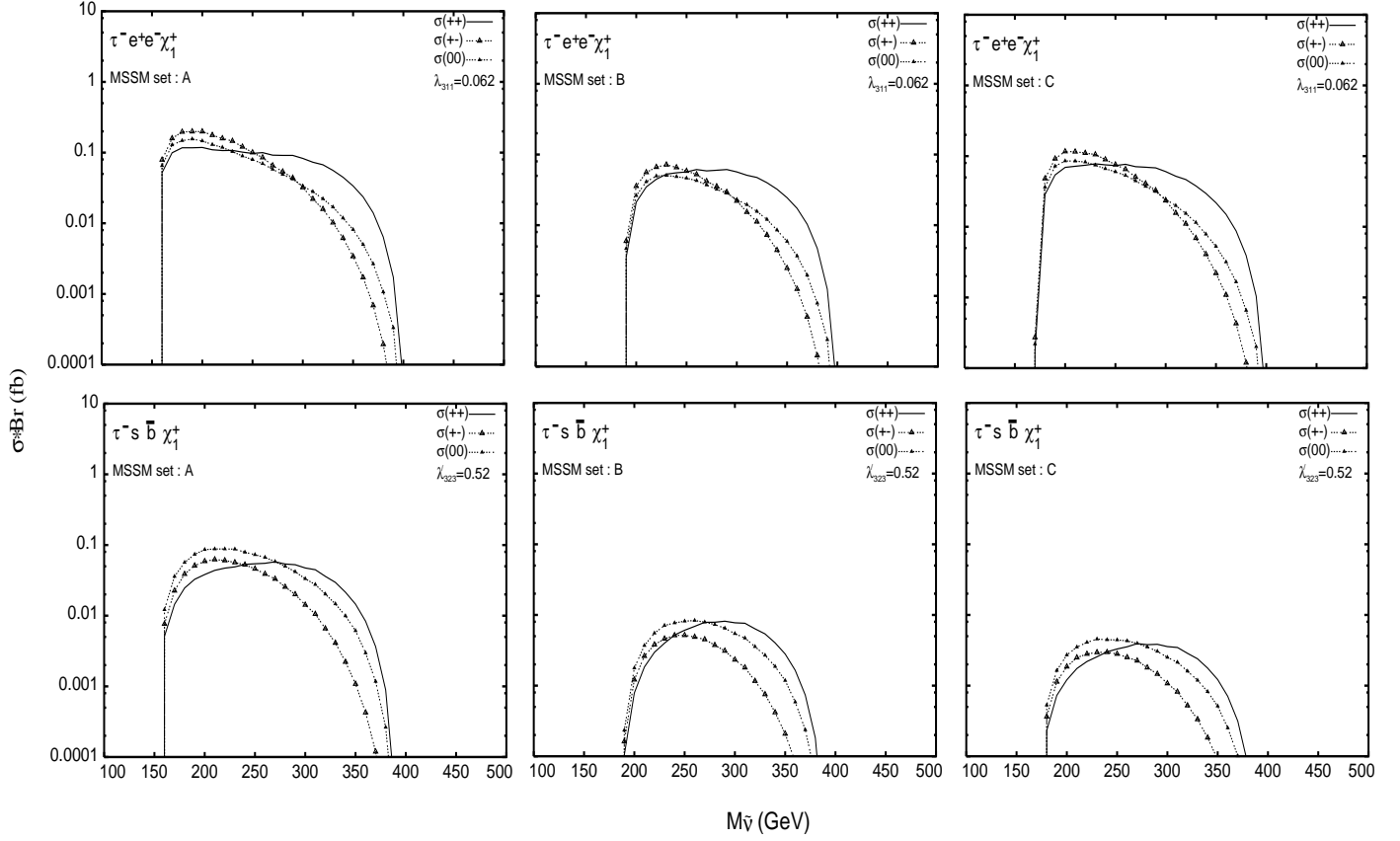


Figure 10: Variation of $\sigma(\gamma\gamma \rightarrow \tilde{\nu}_i f_j \bar{f}_k) * \text{BR}(\tilde{\nu}_i \rightarrow \ell^- \tilde{\chi}_1^+)$ at $\sqrt{s_{e^+e^-}} = 500$ GeV with the sneutrino mass, for fixed values of the relevant λ_{ijk} and λ'_{ijk} couplings. MSSM parameter sets are shown in each figures. Beam polarization conventions are the same as in the previous Figures.